UC Berkeley
UC Berkeley Previously Published Works

Title

A specialized molecular motion opens the Hv1 voltage-gated proton channel

Permalink

Journal

ISSN

Authors

Mony, Laetitia
Berger, Thomas K
Isacoff, Ehud Y

Publication Date

DOI

Peer reviewed

A specialized molecular motion opens the Hv1 voltage-gated proton channel

Laetitia Mony[#1], **Thomas K. Berger**[#1,2], and **Ehud Y. Isacoff**[1,3,4,#]

[1] Department of Molecular and Cell Biology, University of California, Berkeley, CA (USA)

[2] Research Center Caesar, Bonn (Germany)

[3] Helen Wills Neuroscience Institute, University of California, Berkeley, CA (USA)

[4] Physical Bioscience Division, Lawrence Berkeley National Laboratory, Berkeley, CA (USA)

[#] These authors contributed equally to this work.

Summary

The Hv1 proton channel is unique among voltage-gated channels for containing the pore and gate within its voltage-sensing domain (VSD). Opening of the pore has been proposed to include assembly of the selectivity filter between the third arginine (R3) of S4 and an aspartate of S1 (D1). We asked whether gating involves a motion of S1 using *Ciona intestinalis* Hv1. We find that channel opening is concomitant with solution access from the cytoplasm deep into the pore-lining face of S1. Voltage- and patch-clamp fluorometry show that this involves a motion of S1 relative to its surround. S1 motion, and the S4 motion that precedes it, are each influenced by residues on the other helix, suggesting a dynamic interaction between S1 and S4. Our findings suggest that the S1 of Hv1 has specialized to function as part of the channel's gate.

Introduction

Voltage-gated proton channels are expressed in a variety of cell types and tissues. They first have been described in snail neurons[1] and were subsequently found in many different species across phyla, including coccolithophores, amoebozoa, echinoderms, tunicates, and vertebrates[2]. They have important physiological roles, e.g. acid extrusion in lung epithelial cells[3] and sperm[4,5], and regulation of pH homeostasis in phytoplankton[2]. In immune cells, voltage-gated proton channels are involved in charge compensation during reactive oxygen species (ROS) production by the NADPH oxidase complex[6-11]. In microglia, voltage-gated proton channels increase brain damage after ischemic stroke through by assisting the production of ROS[12]. The voltage-gated proton channel Hv1 is a peculiar member of the superfamily of voltage-gated cation channels. "Classical" voltage-gated cation channels are

[#] To whom correspondence should be addressed: ehud@berkeley.edu.

Author contributions

L.M. and T.K.B. performed the experiments and analyzed data. L.M., T.K.B., and E.Y.I designed the experiments and wrote the manuscript.

tetrameric and each subunit contains a voltage-sensing domain (VSD) with transmembrane segments S1 – S4, and a pore domain (PD) that contributes transmembrane segments S5 and S6 and an intervening P region to the central pore[13]. Following its cloning[14,15], it became clear that Hv1, however, has a markedly different architecture. It contains only the VSD, lacking the traditional PD. Hv1 is a dimer[16-18] with a separate pore in each subunit, whose interaction results in cooperative gating[19,20]. The cytosolic C-terminal region contains a coiled coil[21,22] that is necessary for dimerization but not for permeation, and the N-terminal region is also dispensable for proton conduction[16,18]. Moreover, purified Hv1 can be functionally reconstituted in artificial bilayers[17,23], indicating that the VSD contains the channel's voltage sensor, gate, and pore.

As in its tetrameric cousins, the S4 segment of Hv1 moves outward upon membrane depolarization[19]. S4's third voltage-sensing arginine, R3, which enters the membrane at positive voltage[19], is important for proton selectivity[24]. R3 appears to interact with D1 (D112 in human Hv1[24]), an aspartate in the middle of S1 that is unique to Hv1, and critical for proton selectivity[24,25] and selectivity against anions[25]. These findings led to the hypothesis that S4's outward motion places R3 into register with D1 to form the selectivity filter during channel opening (but see ref. 26).

We set out to investigate the role of S1 in gating. We find that a voltage-dependent conformational change that is associated with channel opening increases access of MTS reagents from the internal solution to the face of S1 that contains D1, and therefore faces the pore, until deep into the span of the membrane. Voltage- and patch-clamp fluorometry confirm that S1 moves in relation to its surround with the timing and voltage dependence of the opening transition. This stands in contrast to S4 whose rearrangement precedes opening, as expected for voltage sensing. Our findings indicate that two distinct but interdependent rearrangements involving S1 and S4 take place during the gating process, and suggest that channel opening involves a rearrangement of S1 that opens access for bulk water deep toward the selectivity filter.

Results

S1 accessibility suggests voltage-dependent motion around S1

We tested for voltage-dependent changes of solvent accessibility of S1-cysteine mutants by measuring their rate of modification by membrane-impermeable methane-thiosulfonate (MTS) reagents. The substituted-cysteine accessibility method (SCAM), which assumes that the modification rate by MTS compounds is directly proportional to the solvent accessibility of the introduced cysteine, was previously used to demonstrate that S4 translocates through the membrane during the gating of voltage-dependent ion channels, including Hv1[19,27-29]. In total, we made 29 S1-cysteine mutants of *Ciona intestinalis* Hv1 (CiHv1) (Fig. 1a). We tested external accessibility to MTSET of residues C-terminal of D1 in two-electrode voltage clamp (TEVC) and internal accessibility of residues N-terminal of D1 in excised inside-out patch-clamp recordings.

For residues located at the extracellular end of S1, we used two protocols that kept the channel either 60 % or 10 % of the time at depolarized potential (see Online Methods),

thereby changing the relative time spent in the open and closed state. Wild-type (wt) current ran down by about 10 and 25 % when depolarized 10% and 60 % of the time, respectively (Supplementary Fig. 1a) and showed no effect of exposure to either extracellular MTSES (Supplementary Fig. 1b) or MTSET (Supplementary Fig. 1c). At the external end of S1, only mutants K173C and D171C were affected. External MTSET irreversibly accelerated closure of K173C, but the rate of modification was not significantly state dependent (Fig. 1b-f). The rate of MTS-induced inhibition of D171C was 2.2-fold faster with MTSET (Supplementary Fig. S1d), and 5.5-fold faster with MTSES (Fig. 1g-k) when depolarized 60 % versus 10 % of the time. The differential effect of MTSES and MTSET on D171C may be explained by local differences in surface electrostatics, or by local changes in pH during gating favoring MTSES over MTSET at depolarized potentials[30]. The fact that the two MTS compounds of opposite charge show a voltage-dependence of action nevertheless suggests a slight increase in accessibility around 171 at depolarized potentials.

We next turned to residues located at the intracellular side of S1 (146–159). In inside-out patches, MTSET had no effect on wt channels (Supplementary Fig. 1e), but we detected modification of five cysteine mutants (Fig. 1a). One mutant (H150C) was too inconsistent in behavior to assess state-dependence quantitatively (Supplementary Fig. 1f). MTSET accelerated opening of V151C, I154C, and V157C (Fig. 2a-e and Supplementary Fig. 1g,h) and inhibited I153C (by approximately 70 %, Fig. 2f-h). All four positions showed a very sharp state-dependency, with no or very little modification in the resting state at –80 mV and rapid modification in the open state at +80 mV (Fig. 2 and Supplementary Fig. 1).

In summary, the results suggest that the largest conformational changes around S1 take place at its internal side. Mapping of the internal positions onto the crystal structure of an mHv1-CiVSP-GCN4 chimera[31] (pdb: 3WKV, mHv1cc) reveals that all but position 151 lie on the same face of the helix as D1 in the middle of S1 (Supplementary Fig. 2), suggesting a large structural rearrangement around the VSD internal vestibule[31]. The structural rearrangements around S1 differ from the ones in the region of S4, which undergoes substantial and converse exposure changes at internal and external ends[19].

Environment changes of S1 correlate with channel opening

To identify the functional transition associated with the voltage-dependent change in S1 accessibility, we took advantage of the sharp state-dependence of the 153C modification by MTSET and measured the modification rate at a range of voltages (see Online Methods). The voltage-dependence of the I153C modification rate by MTSET (accessibility-voltage relationship, A-V) was very close to the conductance-voltage relationship (G-V) of the channel before MTS modification (Fig. 3a), suggesting that the increase of accessibility of the internal end of S1 occurs in the opening transition.

Next, we identified the kinetics of the functional transition that changes the environment of S1 using voltage-clamp fluorometry (VCF)[32,33]. A cysteine was introduced at position 175 at the extracellular end of S1 and labeled with the pH-insensitive, environmentally sensitive fluorophore TAMRA-MTS (175C*, Fig. 3b). 175C* showed no fluorescence change (F) in response to hyperpolarizing steps or depolarizing steps that did not open the channel (grey and blue traces in Fig. 3c). In contrast, depolarizing steps that opened the channel gave rise

to a F (green, yellow and red traces in Fig. 3c). This F was caused by TAMRA attached to 175C, since no voltage-induced F was observed for wt channels treated with TAMRA-MTS (Supplementary Fig. 3). The kinetics of the F matched those of the current, both during depolarization-induced activation and repolarization-induced deactivation (Fig. 3d,e). These results suggest that S1 environment changes are associated with opening and closing of the channel gate.

When Hv1 opens, proton flux can modify the local pH and thereby alter gating properties and current kinetics. Even in the presence of high pH buffer content (see ref. 19 and Online Methods), the pH is never perfectly controlled in oocytes. We therefore turned to patch-clamp fluorometry (PCF), which provides a tight control of intra- and extracellular pH, using symmetrical 100 mM HEPES solutions ($pH_{in} = pH_{out} = 7.5$). Giant inside-out patches from fluorescently-labeled oocytes expressing 175C* were voltage clamped and simultaneously imaged by a CCD camera (Fig. 4a). As in VCF, only voltage steps that were large enough to open the channel evoked a F (Fig. 4a). The steady-state fluorescence-voltage (F-V) relationship closely tracked the G-V relationship (Fig. 4b). Moreover, the kinetics of the F and current matched during both activation and deactivation for different voltages (Fig. 4c,d). Together, the results show that channel opening and closure is concomitant with a change in TAMRA fluorescence at the outer end of S1.

Although the TAMRA fluorophore has been reported to have little pH sensitivity, we verified that the proton flux itself did not contribute to F. Therefore, we tested whether a block of proton efflux affects F. In 175C*, we introduced a cysteine at position N264, which lies at the fourth position of the S4 arginine repeat (Supplementary Fig. 4a). Modification of the equivalent position in hHv1 (N214) by MTSET blocks most of the proton current, while leaving the residual G-V relationship unchanged[18]. Similarly to hHv1-N214C, 1 mM MTSET reduced proton current of 175C*-N264C channels by approximately 90 % ($I_{after\ MTSET}/I_{before\ MTSET} = 0.11 \pm 0.02$, Supplementary Fig. 4b,c). In contrast, the F amplitude was almost unchanged after MTSET treatment ($F_{after\ MTSET}/F_{before\ MTSET} = 0.91 \pm 0.05$, Supplementary Fig. 4b,c), indicating that the F at 175C* is caused by conformational changes of the channel, not by proton flux.

To confirm that the conformational changes tracked at the external end of S1 represent the opening and closing transitions, we perturbed channel gating by mutating aspartate D1 (D160) to a glutamate and analyzed the effect on the F at 175C*. In hHv1, mutation of D1 into a glutamate does not disrupt proton selectivity[25], but slows channel closure[24]. Similarly, the D1E mutation in the 175C* background slowed deactivation by a factor of 4, while barely affecting the activation time constants (Supplementary Fig. 4d-f). The fluorescence kinetics changed by the same amount and a good match between current and fluorescence kinetics in D1E-175C* remained (Supplementary Fig. 4e,f). Thus, a structural rearrangement around S1 accompanies the opening and closing steps.

S1 undergoes voltage-dependent motion

Do the changes in fluorescence and solution accessibility reflect a rearrangement of S1 itself, or are they indirect consequences of motion of another part of the protein, such as S4? While S4 undergoes a major transmembrane motion that displaces gating charge[19,34], it has

also been proposed to undergo a conformational change during opening[35], raising the possibility that environment changes monitored at S1 may indirectly report S4 motion. If S1 itself underwent a rearrangement during the gating step, Fs tracking the gating step should be observed at several attachment sites pointing to different directions on S1. Position 173C labeled with Alexa488-maleimide (173C-Alexa) gave sufficient Fs to permit detailed analysis. 173C-Alexa Fs contained two main components: a very fast component (F_{fast}) occurring during the depolarization- and repolarization-induced capacitive transients, and a slower fluorescence component (F_{slow}) (Supplementary Fig. 5a-c). While F_{fast} was faster than channel opening and closure and occurred at potentials hyperpolarized to channel opening (Supplementary Fig. 5c,d), F_{slow} had kinetics and voltage-dependence that matched channel gating (Supplementary Fig. 5d-i). According to the mHv1cc crystal structure, K173 points away from the VSD, while I175 is predicted to point towards the interior of the VSD[31]. Thus, at least two positions of the S1 segment pointing in different directions (and thus pointing towards different environments), 173 and 175, can track the gating transition. This supports the hypothesis that the Fs at these positions reflect an S1 motion, rather than changes of the environments to which the fluorophores point.

To examine S1 rearrangement in a more direct fashion, we considered an intriguing implication of a putative S1 motion. In the dimer, the outer end of S1 is close enough to the other subunit's S1 to disulfide bond[17]. Therefore, an S1 motion would change S1-S1 distance or orientation. Tryptophans quench the fluorescence of organic fluorophores in a distance- or orientation-dependent manner through electron transfer from the tryptophan side-chain to the excited state of the fluorophore[36-38]. As a consequence, tryptophan-induced amplitude changes of a dye fluorescence can be used to study structural rearrangements in proteins, as was previously shown in other ion channels[39,40]. We constructed tandem dimers with only one subunit containing a cysteine at position 174, at the external end of S1, and labeled it with TAMRA-MTS (174C*). In tandem dimers in which the 174C* subunit faced a wt subunit (wt-td-174C*), no F was detected during a voltage step to +100 mV (Fig. 5a). In contrast, when the 174C* subunit faced a subunit with a tryptophan introduced at position V174W in S1 (V174W-td-174C*), a clear F was observed in response to a +100 mV step voltage ($F/F = -1.3 \pm 0.3$ %, Fig. 5a,b). Since wt-td-174C* channels are fluorescently silent, the F of V174W-td-V174C* reflects quenching of TAMRA by the tryptophan at depolarized potentials. We thus find that the external ends of the two S1 segments in the dimer move relative to each other following membrane depolarization, indicating that S1 does indeed undergo a structural rearrangement.

S1 and S4 undergo distinct motions and influence one another

Next, we tracked S4 motion with TAMRA-MTS at position 249 using PCF (Fig. 6a). Hyperpolarization increased fluorescence, while depolarization decreased fluorescence (Fig. 6b). The F-V curve was negatively shifted compared to the conductance-voltage (G-V) curve (Fig. 6c). In addition, the F took place during the fast current component (fluorescence τ_{on} = 12 ± 6 ms vs current fast τ_{on} = 21 ± 9 mV at +40 mV, Fig. 6d), and, thus, was overall faster than channel opening. A similar F preceding gating kinetically and thermodynamically was also observed at the nearby position 242C (see Supplementary Fig. 6 and refs 19,35), consistently with Fs at 242C and 249C tracking the voltage-sensing

rearrangement of S4. This is in contrast to the structural changes in the S1 region which track opening both kinetically and in voltage dependence.

Mutants of selectivity-filter residues D1 and R3 further distinguished S1 and S4 motions. In VCF, double-mutant neutralization D1N-R3S slowed F deactivation kinetics only at 249C* but not at 175C* (Fig. 7a-d). In addition, D1N-R3S-175C* showed a rightward shift of both F-V and G-V relationships compared to 175C*, preserving a close match between the F-V and G-V in the mutant (a further confirmation that 175C* fluorescence tracks gating, Supplementary Fig. 7a). In contrast, the discrepancy between the voltage-dependences channel opening and S4 motion increased for D1N-R3S-249C* as compared to 249C* (Supplementary Fig. 7b). These results further support the interpretation that the F observed at 175C* does not reflect a motion of S4, but a distinct conformational change of S1 that is associated with gating.

While S1 and S4 seem to move together during deactivation in the wt background (S1 and S4 Fs both have off-rates similar to the tail current), their kinetics differ in the D1N-R3S background (Fig. 7c,d and Supplementary Fig. 7c,d). By neutralizing the selectivity-filter residues, we were thus able to decouple S1 and S4 motions during repolarization. We furthermore found that mutating R3 to serine induced a slight acceleration of deactivation F (F_{off}) for the S1 labeling site (175C*) (by about 2-fold, Supplementary Fig. 7e,f) and shifted the F-V by around +20 mV to the right (Supplementary Fig. 7a). In the D1N-175C* background, however, the R3S mutation accelerated F_{off} by 50-fold (compare the τ_{off} of D1N-175C* and D1N-R3S-175C* in Fig. 7 and Supplementary Fig. 7f), suggesting an interaction between D1 and R3 in the active state. Neutralization of D1 slowed the fast component of the F_{off} of the S4 labeling site (249C*) by approximately 8-fold, introduced a brightening component to the dimming F_{on} (Supplementary Fig. 7g,h), and increased the steepness of the voltage-dependence of 249C* fluorescence signal (Supplementary Fig. 7b). Since, as shown above, S4 deactivation motion seems to be limited by S1 motion in the wt (Supplementary Fig. 7a), slowing of 249C* F_{off} by the D1N mutation may be indirectly due to its slowing of S1 motion (by approximately 60-fold in the 175C* background, Supplementary Fig. 7e), thus reinforcing the idea of an interaction between S1 and S4 in the active state. These results suggest that interaction between S1 and S4 via their selectivity filter residues D1 and R3 mutually influences their motions.

Discussion

The Hv1 proton channel is unique because its VSD contains the channel's voltage sensor, gate, and pore. A depolarization-driven outward motion of S4 has been proposed to trigger a subsequent rearrangement that opens the channel[19,20,24,35,41]. Using cysteine-accessibility analysis and fluorometry we show that channel opening also involves a rearrangement of S1, whose unique D1 lines the selectivity filter in the pore[24,25].

Several lines of evidence suggest that the state-dependent change in environment around S1 is caused by a structural rearrangement in S1 itself: 1) At S1 position I153C, the accessibility-voltage relationship closely tracked the conductance-voltage relationship, indicating that the rearrangement that changes the environment around S1 is associated with

the opening transition. 2) In agreement with (1), fluorometry showed that the voltage dependence and kinetics of the structural rearrangement around the outer end of S1 occurs during the opening and closure of the channel. 3) In contrast, the rearrangement around the outer end of S4 preceded channel opening kinetically and occurred at more negative voltage. 4) The association between S1 fluorescence change and channel opening was maintained when gating was perturbed by mutations, whereas S4 fluorescence change was further dissociated from the open–closed transition. 5) Fluorescence quenching between a fluorophore attached to S1 in one subunit and a tryptophan introduced into the S1 of the other subunit revealed a voltage-dependent change in quenching that indicates a relative motion of the two S1 segments in the dimer. Together, accessibility and fluorometry results suggest that opening–closing of the gate of Hv1 involves a structural rearrangement of S1.

The four positions near the internal end of S1, which become more accessible to the internal solution at positive voltage, span the internal half of S1 and reach from the inside up to one helical turn before D1 (Supplementary Fig. 2), suggesting that S1 motion opens a deep internal crevice when the channel opens. Three of these residues, 153, 154 and 157, are located on the same face of the helix as selectivity residue D1[31] (Supplementary Fig. 2), and so, like D1, are predicted to face the lumen of the open pore. Thus, channel opening appears to be accompanied by a rearrangement that opens solution access to the selectivity filter (Fig. 7e and Supplementary Fig. 8a). This could account for the selective open-state entry of bulky guanidinium blockers from the internal solution into the pore[41,42].

The mHv1cc crystal structure was proposed to capture a closed state, based on the presence of Zn^{2+} at the external site whose occupancy favors closure[31]. The structure "already" has an internal vestibule, which is, however, too narrow to allow MTSET to reach cysteine at position 157, located in the lower hydrophobic plug, along with F198 and F230[31,43,44]. Although the pathway to positions 154 and 153 is wide enough to accommodate water in the crystal structure (Supplementary Fig. 8b,c), these residues are surrounded by I206, I262 and H150 that could hinder MTSET access (Supplementary Fig. 8c,d). This may also be the reason why docking of guanidinium blockers is hindered in the closed state[42]. Finally, position 151 points away from the VSD, but is likely to either take part of the dimer interface, or be buried in the membrane in membrane-embedded dimeric channels, thus being inaccessible to water-soluble MTS compounds. We therefore propose that, following the voltage-sensing outward motion of S4, the channel opens *via* a motion that includes a rearrangement of S1 with respect to its surround, which widens the internal vestibule and thereby allows for solution access from the cytoplasm to the selectivity filter to enable proton flux (Fig. 7e and Supplementary Fig. 8a).

Depolarization induced a drastic increase in accessibility in the internal side of S1, but only mildly affected the accessibility at one site at the external side of S1. Still, this rearrangement at the external end of S1 was sufficient to generate an inter-S1 change in the dimer that was detected as a tryptophan quenching change. Thus, S1 appears to undergo a motion relative to its surround that pivots near its external end so that a larger rearrangement occurs at its internal end (Fig. 7e and Supplementary Fig. 8a). This is in contrast to the voltage-sensing motion of S4, whose outward transmembrane displacement by depolarization induces drastic and opposite changes of exposure at its internal and external

ends[19], as seen in Kv and Nav channels[27,28,45,46]. The mechanism that drives S1 motion still needs to be determined. S1 contains three negatively charged residues (D1, E167 and D171) that could move inward at positive voltage and therefore carry some gating charge[43]. However, the gating charge of Hv1 appears to be mostly contained in the arginines of S4[34], suggesting that S1 motion is a consequence of the voltage-dependent rearrangement of S4.

The gating rearrangement at the external end of S1 might contribute to inter-subunit cooperativity[19,20]. S1 motion during the opening of one of the subunits would be expected to influence S1 motion, and thus opening, of the other subunit, as suggested recently by the influence of a mutation at the outer end of S1 on a cooperative rearrangement tracked by S4[35].

While in classical tetrameric voltage-gated channels S1 also appears to interact with S4[47-50], the function and interactions of S1 in the dimeric Hv1 channel have differentiated from these channels. The S1 of Kv channels interacts with S5 and the pore helix[51,52], which are absent in Hv1. In tetrameric channels there is no contact between VSDs, while the S1 of Hv1 lies at the dimer interface between the VSDs[17]. Nevertheless, earlier voltage-clamp fluorometry on the Shaker Kv channel revealed a fast rearrangement in S1, although it was not resolved whether this corresponds to the voltage-sensing or opening steps[53]. The monomeric voltage-sensing phosphatase (VSP) also undergoes voltage-dependent conformational changes in S1[54]. However, in VSP, S1 and S4 fluorescence signals have similar properties, consistent with participation in a common conformational step, in contrast to what we find here for Hv1. Thus, Hv1 seems to have a unique and specialized gating motion of S1 that allows access to the deep pore of the channel and enables proton flux through its VSD.

Online Methods

Mutagenesis and expression in *Xenopus* oocytes

Female *Xenopus laevis* animals were housed and surged according to the guidelines of Berkeley's Animal Care and Use Committee (ACUC) (Animal Use Protocol R187-0814). In some cases, *Xenopus laevis* oocytes were purchased (Ecocyte, Castrop-Rauxel, Germany). CiHv1 mutants were constructed via site-directed mutagenesis in the pSD64TF vector[15] using Quikchange mutagenesis (Stratagene, La Jolla, CA) and verified by sequencing. DNA was linearized with SbfI and transcribed to RNA using the SP6 mMessage mMachine Kit (Ambion, Texas, TX). *Xenopus laevis* oocytes were injected with 50 nL of RNA at a concentration of 0.5-2 µg/µL and incubated at 18 °C for 1-5 days in ND96 containing (in mM): 96 NaCl, 2 KCl, 1.8 CaCl$_2$, 1 MgCl$_2$, 10 HEPES, 5 pyruvate, and 100 mg/L gentamycin, pH = 7.6. CiHv1 tandem dimers contained a 17-long amino-acid linker between the two Hv1 monomers with the sequence GGSGGSGGSGGSGGSGG and were generated according to ref. 18.

Cysteine accessibility measurements in TEVC and patch-clamp recordings

Cysteine accessibility experiments to methane thiosulfonate (MTS) reagents were performed in TEVC and excised inside-out patch clamp. TEVC recordings were adapted from different

protocols[19,20]. To minimize pH changes due to proton efflux, high buffer solutions (100 mM HEPES) were used both intra- and extracellularly. On the day of the experiment, oocytes were injected with 50 nL of a solution of 1 M of 2-(4-(2-hydroxyethyl)piperazin-1-yl)ethanesulfonic acid (HEPES) at pH 7.0 (pH adjusted to 7.0 with KOH) and left 1-2 h at 18 °C to recover in the extracellular recording solution. This results in approximately 100 mM HEPES in the cytosol[19]. The extracellular recording solution contained (in mM): 46 NaCl, 1 KCl, 1 $MgCl_2$, 1 $CaCl_2$, 100 HEPES, pH adjusted to 7.5 with NaOH. Patch-clamp recordings were performed using symmetric pipette (extracellular) and bath (intracellular) solutions void of metallic cations containing (in mM) 100 HEPES, 30 methanesulfonic acid (MS), 5 tetraethylammonium chloride (TEACl), 5 ethylene glycol-bis(2-aminoethylether)-N,N,N',N'-tetraacetic acid (EGTA), adjusted to pH 7.0 with TEA hydroxide (>25 mM).

[2-(trimethylammonium)ethyl]methanethiosulfonate bromide (MTSET) and Sodium (2-sulfonatoethyl)methanethiosulfonate (MTSES) were purchased from Toronto Research Chemicals (North York, ON) and stored as powder at −20 °C. On the day of the experiment, MTS powder was diluted in water to form stock solutions of 100 or 500 mM concentrations and stored at 0 °C. The stock solutions were then diluted in the recording media to the final concentration of 1 mM (H150C, I153C, I154C, and D171C), 0.5 mM (V157C), 200 μM (V151C), or 100 μM (K173C). To avoid variations of MTS concentration due to hydrolysis, final solutions were prepared fresh just before each recording and kept 15 min maximum.

Extracellular cysteine accessibility to MTS reagents of the S1 segment was tested by TEVC ($pH_{in} \approx 7$, $pH_{out} = 7.5$). Intracellular accessibility was tested by patch-clamp in the inside-out configuration ($pH_{in} = pH_{out} = 7$). Holding potential was −80 mV. Irreversible, steady-state effects of MTS compounds were calculated by dividing current amplitude after application and washout of the MTS by the current amplitude before MTS application. State-dependence of MTS reaction was tested using different protocols that vary the proportion of time that channels spend in the open state during MTS application. D171C and K173C mutants (TEVC) were repeatedly depolarized to +60 mV (open state) during 3 s, then repolarized to −80 mV during either 2 s (60 % at +60 mV) or 27 s (10 % at +60 mV). State-dependence of the MTSET effect on internally located sites (in patch-clamp experiments) was probed by comparing currents elicited by a voltage step to +80 mV before and after treatment with MTSET, either at −80 mV (closed state), or during repeated steps to +80 mV (open state), and washout. Rate constants of MTSET modification (k_{MTSET}) at +80 mV on I153C (as shown in Fig. 2) were calculated by directly fitting the current decrease during the depolarization step to +80 mV in presence of MTSET. For all other cysteine mutants, for which MTSET induced an acceleration of channel opening, rate constants of MTS effect at +80 mV were calculated by plotting the amplitude of the current (time point indicated by an arrowhead in Fig. 1, 2 and S1) against the time spent in MTS at +80 mV. Time constants of MTS (τ_{MTS}) inhibition were obtained from the single exponential fits of the individual "current" vs. "time in MTS" curves and the rate constants calculated assuming a pseudo first-order reaction: $k_{MTS} = 1/(\tau_{MTS}*[MTS])$. The rate constants of MTS effect at −80 mV were approximated by the slope of a linear fit between the current amplitudes before MTS application (at −80 mV) and after MTS washout, normalized by the current amplitude after complete MTS modification at +80 mV. MTS-induced maximal

inhibition was defined as the ratio of the current amplitude after washing out MTS by the current measured before MTS application at the time point indicated by an arrowhead.

Modification of 153C channels by MTSET induces a shift of the G-V relationship by approximately −60 mV, so that in many patches the modified channels are open at the −80 mV holding potential. Voltage-dependence of MTSET action at position 153C (Fig. 3) was determined by measuring the rate of current increase at the holding potential, as a readout of the number of modified channels, while constantly stepping to a determined voltage for 1 s every 1 s. This method enabled us to measure the rate of channel modification even for potentials that do not fully open the unmodified channel.

VCF recordings

VCF recordings were adapted from previously described protocols[19,20,33,55]. Similarly to TEVC experiments, oocytes were injected ≈ 1-2 h prior to recording with a 1 M HEPES solution at pH 7.0 to obtain ≈ 100 mM HEPES intracellularly. Oocytes were then labeled for 45 min to 1 h in ice with 50 μM of 2-((5(6)-tetramethylrhodamine) carboxylamino) ethyl methanethiosulfonate (TAMRA-MTS, Toronto Research Chemicals) for 175C, or AlexaFluor488-C_5-maleimide (Thermo Fisher Scientific, Waltham, MA) for 173C, diluted in the extracellular recording solution used in TEVC. Previous studies showed that S4 residues starting from A246 are more accessible at depolarized potentials[19]. To increase the accessibility of the introduced cysteine at position 249, a solution with a higher potassium content (in mM: 46 NaCl, 1 KCl, 1 $MgCl_2$, 1 $CaCl_2$, and 100 HEPES, pH adjusted to 7.5 with KOH [approximately 50 mM]) was used to label 249C channels with TAMRA-MTS. After labeling, oocytes were extensively washed in the recording solution and stored in the dark at +18 °C during the course of the experiment. Chemicals were bought from Sigma-Aldrich (St. Louis, MO) or Thermo Fischer Scientific.

TEVC recordings were done with a Dagan CA-1 amplifier (Dagan, Minneapolis, MN). Fluorescence signals were acquired through a 20x, 0.75-NA fluorescence objective (Nikon, Tokyo, Japan) on a Nikon Diaphot inverted microscope illuminated with a 150 W xenon lamp. Light was filtered through an HQ535/50 excitation filter, an HQ610/75 emission filter and a Q565LP dichroic (Chroma Technology, Bellows Falls, VT). Fluorescence intensity was measured with a Hamamatsu HC120-05 photomultiplier tube. Fluorescence signals were low-pass filtered at 2 kHz through an eight-pole Bessel filter (Frequency Devices, Ottawa, IL) and sampled at 10 kHz through a Digidata-1440A controlled by pClamp 10 (Molecular Devices, Union City, CA). Holding potential was −80 mV. Unless specified, fluorescence and current traces are the average of three recordings successively measured on the same oocyte and filtered with a boxcar filter (box width 55 approximately equivalent to a cutoff frequency of 500 Hz). Currents were leak-subtracted off line, assuming ohmic leak and using currents from potentials between −80 and −40 mV. Fluorescence signals were normalized to the baseline level to obtain F/F values.

PCF recordings

For PCF recordings, oocytes were labeled on ice without prior HEPES injection on the day of recording with 50 μM TAMRA-MTS in (in mM) 92 KCl, 0.75 $CaCl_2$, 1 $MgCl_2$, 10

HEPES; pH adjusted to pH 7.5 with KOH. Before recordings, oocytes were mechanically devitellinated under a stereoscope, and placed in a recording chamber under an inverted IX71 microscope (Olympus, Tokyo, Japan). Giant patch electrodes were pulled from G150TF-4 capillaries (Warner Instruments, Hamden, CT) on a P97 Micropipette Puller (Sutter, Novato, CA) and extensively fire polished on a microforge (Narishige MF-83, Tokyo, Japan). Excised patches in the inside-out configuration were obtained under a 20x objective with an initial electrode resistance of 0.6–2 MΩ, depending on the pipette solution. After establishing the excised patch the objective was changed (Olympus PLAPON 60XOTIRFM NA1.45) for recording and imaging. Holding potentials were −60 or −80 mV. Recordings were performed at room temperature (22 °C–25 °C), with an Axopatch 200B or 200A amplifier (Molecular Devices), connected via a Digidata 1440A acquisition board to a PC running pClamp 10 (Molecular Devices). Data were filtered at 2 or 5 kHz and the sampling rate was 10 kHz. Symmetric pipette (extracellular) and bath (intracellular) solutions were the same as in patch-clamp recordings, but titrated to pH 7.5. Polychrome V (TILL Photonics, Gräfelfing, Germany), attenuated by a neutral density filter (ND 1), or Lumencor Spectra (Lumencor, Beaverton, OR) were used as a light source. A TRITC cube (excitation filter FF01-542/20-25, dichroic FF570-Di01-25x36, emission filter FF01-620/52-25, Semrock, Rochester, NY) was used for imaging. Fluorescent signals were acquired with an emCCD camera (Luca S or iXon Ultra, Andor Technologies, Belfast, UK). We recorded a rectangular region of interest with 4x4 or 8x8 binning in the frame transfer mode, allowing frame rates of 0.2 kHz. The spatial average of the region of interest containing the patch cone (see Fig. 5A and 7A) was taken as the fluorescence signal. For fitting purposes, the signal was either left unfiltered or, for one patch, filtered with a boxcar filter (box width 3). For display purposes, the signal was filtered with a boxcar filter of box width 7.

Data analysis and statistics

All the values in the paper represent average values. Error bars represent the standard error of the mean (SEM). "n" represents the number of oocytes or patches tested. Data were collected on at least two different experimental days, on oocytes obtained from at least two different *Xenopus*. Before running statistical tests, sample distributions were tested for normality using the Kolmogorov-Smirnov test. All Student's and paired t-tests are two-sided, with samples considered of unequal variance.

Data were analyzed using Clampfit (Molecular Devices), Igor Pro (WaveMetrics, Portland, OR), SigmaPlot (Systat Software, San Jose, CA) and Matlab (Mathworks, Natick, MA) software. Activation time constants of current and fluorescence, as well as deactivation time constants of fluorescence and current traces of 249C* mutants, were determined by fitting the current and fluorescence traces with a bi-exponential function in the form: I (or F) = $A_{fast}*\exp(-t/\tau_{fast}) + A_{slow}*\exp(-t/\tau_{slow})$, where τ_{fast} and τ_{slow} represent the time constants of the fast and the slow components, respectively, and A_{fast} and A_{slow} the amplitudes of the fast and slow components, respectively. VCF deactivation fluorescence signal of 249C* had a fast component that matched the current kinetics (see (d)), as well as a small, very slow component that was absent in PCF experiments. We therefore took into consideration only the fast component of fluorescence recovery for 249C* and compared it to the fast

component of tail current. Deactivation fluorescence and current traces of 175C* mutants were best fitted with single exponential functions. In VCF experiments, the tail currents of D1E-175C* and 173C-Alexa had slow kinetics and a bumpy shape (possibly due to imperfect clamping) that made it difficult to fit them. To quantify the rate of tail current and fluorescence decrease for these channels, we measured the tail decay time, defined as the time necessary for current or fluorescence to decay from 90 to 10 % of their initial amplitude following repolarization to –80 mV.

G-V curves were calculated from the tail current amplitudes at –80 mV. Unless specified, *F-V* curves were calculated from the amplitudes of fluorescence changes at the end of each voltage step. *G-V* and *F-V* curves were fitted using the Boltzmann equation: G/G_{max} (or $F/F_{max}) = 1 / (1 + \exp(-ze_0/(kT)*(V-V_{1/2}))$, where z is the number of elementary charges, e_0 the elementary charge, k the Boltzmann's constant, T the absolute temperature, and $V_{1/2}$ the voltage at which half of the channels are open.

Structure Illustration

Structure representations were prepared with Discovery Studio 4.0 (Accelrys, San Diego, CA).

Supplementary Material

Refer to Web version on PubMed Central for supplementary material.

Acknowledgments

References

1. Thomas RC, Meech RW. Hydrogen ion currents and intracellular pH in depolarized voltage-clamped snail neurones. Nature. 1982; 299:826–8. [PubMed: 7133121]

2. Taylor AR, Chrachri A, Wheeler G, Goddard H, Brownlee C. A Voltage-Gated H+ Channel Underlying pH Homeostasis in Calcifying Coccolithophores. Plos Biology. 2011; 9

3. Iovannisci D, Illek B, Fischer H. Function of the HVCN1 proton channel in airway epithelia and a naturally occurring mutation, M91T. J Gen Physiol. 2010; 136:35–46. [PubMed: 20548053]

4. Lishko PV, Botchkina IL, Fedorenko A, Kirichok Y. Acid extrusion from human spermatozoa is mediated by flagellar voltage-gated proton channel. Cell. 2010; 140:327–37. [PubMed: 20144758]

5. Lishko PV, et al. The control of male fertility by spermatozoan ion channels. Annu Rev Physiol. 2012; 74:453–75. [PubMed: 22017176]

6. Capasso M, et al. HVCN1 modulates BCR signal strength via regulation of BCR-dependent generation of reactive oxygen species. Nat Immunol. 2010; 11:265–72. [PubMed: 20139987]

7. El Chemaly A, et al. VSOP/Hv1 proton channels sustain calcium entry, neutrophil migration, and superoxide production by limiting cell depolarization and acidification. J Exp Med. 2010; 207:129–39. [PubMed: 20026664]

8. Henderson LM, Chappell JB, Jones OT. The superoxide-generating NADPH oxidase of human neutrophils is electrogenic and associated with an H+ channel. Biochem J. 1987; 246:325–9. [PubMed: 2825632]

9. Ramsey IS, Ruchti E, Kaczmarek JS, Clapham DE. Hv1 proton channels are required for high-level NADPH oxidase-dependent superoxide production during the phagocyte respiratory burst. Proc Natl Acad Sci U S A. 2009; 106:7642–7. [PubMed: 19372380]

10. Reth M, Dick TP. Voltage control for B cell activation. Nat Immunol. 2010; 11:191–2. [PubMed: 20157299]

11. Sasaki M, et al. Autoimmune disorder phenotypes in Hvcn1-deficient mice. Biochem J. 2013; 450:295–301. [PubMed: 23231444]

12. Wu LJ, et al. The voltage-gated proton channel Hv1 enhances brain damage from ischemic stroke. Nat Neurosci. 2012; 15:565–73. [PubMed: 22388960]

13. Tombola F, Pathak MM, Isacoff EY. How does voltage open an ion channel? Annu Rev Cell Dev Biol. 2006; 22:23–52. [PubMed: 16704338]

14. Ramsey IS, Moran MM, Chong JA, Clapham DE. A voltage-gated proton-selective channel lacking the pore domain. Nature. 2006; 440:1213–6. [PubMed: 16554753]

15. Sasaki M, Takagi M, Okamura Y. A voltage sensor-domain protein is a voltage-gated proton channel. Science. 2006; 312:589–92. [PubMed: 16556803]

16. Koch HP, et al. Multimeric nature of voltage-gated proton channels. Proc Natl Acad Sci U S A. 2008; 105:9111–6. [PubMed: 18583477]

17. Lee SY, Letts JA, Mackinnon R. Dimeric subunit stoichiometry of the human voltage-dependent proton channel Hv1. Proc Natl Acad Sci U S A. 2008; 105:7692–5. [PubMed: 18509058]

18. Tombola F, Ulbrich MH, Isacoff EY. The voltage-gated proton channel Hv1 has two pores, each controlled by one voltage sensor. Neuron. 2008; 58:546–56. [PubMed: 18498736]

19. Gonzalez C, Koch HP, Drum BM, Larsson HP. Strong cooperativity between subunits in voltage-gated proton channels. Nat Struct Mol Biol. 2010; 17:51–6. [PubMed: 20023639]

20. Tombola F, Ulbrich MH, Kohout SC, Isacoff EY. The opening of the two pores of the Hv1 voltage-gated proton channel is tuned by cooperativity. Nat Struct Mol Biol. 2010; 17:44–50. [PubMed: 20023640]

21. Fujiwara Y, et al. The cytoplasmic coiled-coil mediates cooperative gating temperature sensitivity in the voltage-gated H(+) channel Hv1. Nat Commun. 2012; 3:816. [PubMed: 22569364]

22. Li SJ, et al. The role and structure of the carboxyl-terminal domain of the human voltage-gated proton channel Hv1. J Biol Chem. 2010; 285:12047–54. [PubMed: 20147290]

23. Lee SY, Letts JA, MacKinnon R. Functional reconstitution of purified human Hv1 H+ channels. J Mol Biol. 2009; 387:1055–60. [PubMed: 19233200]

24. Berger TK, Isacoff EY. The pore of the voltage-gated proton channel. Neuron. 2011; 72:991–1000. [PubMed: 22196334]

25. Musset B, et al. Aspartate 112 is the selectivity filter of the human voltage-gated proton channel. Nature. 2011; 480:273–7. [PubMed: 22020278]

26. Sakata S, et al. Functionality of the voltage-gated proton channel truncated in S4. Proc Natl Acad Sci U S A. 2010; 107:2313–8. [PubMed: 20018719]

27. Larsson HP, Baker OS, Dhillon DS, Isacoff EY. Transmembrane movement of the shaker K+ channel S4. Neuron. 1996; 16:387–97. [PubMed: 8789953]

28. Yang N, George AL Jr. Horn R. Molecular basis of charge movement in voltage-gated sodium channels. Neuron. 1996; 16:113–22. [PubMed: 8562074]

29. Yusaf SP, Wray D, Sivaprasadarao A. Measurement of the movement of the S4 segment during the activation of a voltage-gated potassium channel. Pflugers Arch. 1996; 433:91–7. [PubMed: 9019737]

30. Elinder F, Mannikko R, Larsson HP. S4 charges move close to residues in the pore domain during activation in a K channel. J Gen Physiol. 2001; 118:1–10. [PubMed: 11429439]

31. Takeshita K, et al. X-ray crystal structure of voltage-gated proton channel. Nat Struct Mol Biol. 2014

32. Cha A, Bezanilla F. Characterizing voltage-dependent conformational changes in the Shaker K+ channel with fluorescence. Neuron. 1997; 19:1127–40. [PubMed: 9390525]

33. Mannuzzu LM, Moronne MM, Isacoff EY. Direct physical measure of conformational rearrangement underlying potassium channel gating. Science. 1996; 271:213–6. [PubMed: 8539623]

34. Gonzalez C, Rebolledo S, Perez ME, Larsson HP. Molecular mechanism of voltage sensing in voltage-gated proton channels. J Gen Physiol. 2013

35. Qiu F, Rebolledo S, Gonzalez C, Larsson HP. Subunit Interactions during Cooperative Opening of Voltage-Gated Proton Channels. Neuron. 2013; 77:288–98. [PubMed: 23352165]

36. Doose S, Neuweiler H, Sauer M. Fluorescence quenching by photoinduced electron transfer: a reporter for conformational dynamics of macromolecules. Chemphyschem. 2009; 10:1389–98. [PubMed: 19475638]

37. Mansoor SE, Dewitt MA, Farrens DL. Distance mapping in proteins using fluorescence spectroscopy: the tryptophan-induced quenching (TrIQ) method. Biochemistry. 2010; 49:9722–31. [PubMed: 20886836]

38. Mansoor SE, McHaourab HS, Farrens DL. Mapping proximity within proteins using fluorescence spectroscopy. A study of T4 lysozyme showing that tryptophan residues quench bimane fluorescence. Biochemistry. 2002; 41:2475–84. [PubMed: 11851393]

39. Islas LD, Zagotta WN. Short-range molecular rearrangements in ion channels detected by tryptophan quenching of bimane fluorescence. J Gen Physiol. 2006; 128:337–46. [PubMed: 16940556]

40. Pantazis A, Kohanteb AP, Olcese R. Relative motion of transmembrane segments S0 and S4 during voltage sensor activation in the human BK(Ca) channel. J Gen Physiol. 2010; 136:645–57. [PubMed: 21078868]

41. Hong L, Pathak MM, Kim IH, Ta D, Tombola F. Voltage-sensing domain of voltage-gated proton channel hv1 shares mechanism of block with pore domains. Neuron. 2013; 77:274–87. [PubMed: 23352164]

42. Hong L, Kim IH, Tombola F. Molecular determinants of Hv1 proton channel inhibition by guanidine derivatives. Proc Natl Acad Sci U S A. 2014; 111:9971–6. [PubMed: 24912149]

43. Chamberlin A, et al. Hydrophobic plug functions as a gate in voltage-gated proton channels. Proc Natl Acad Sci U S A. 2014; 111:E273–82. [PubMed: 24379371]

44. Kurokawa T, Okamura Y. Mapping of sites facing aqueous environment of voltage-gated proton channel at resting state: A study with PEGylation protection. Biochim Biophys Acta. 2013

45. Baker OS, Larsson HP, Mannuzzu LM, Isacoff EY. Three transmembrane conformations and sequence-dependent displacement of the S4 domain in shaker K+ channel gating. Neuron. 1998; 20:1283–94. [PubMed: 9655514]

46. Yang N, Horn R. Evidence for voltage-dependent S4 movement in sodium channels. Neuron. 1995; 15:213–8. [PubMed: 7619524]

47. Henrion U, et al. Tracking a complete voltage-sensor cycle with metal-ion bridges. Proc Natl Acad Sci U S A. 2012; 109:8552–7. [PubMed: 22538811]

48. DeCaen PG, Yarov-Yarovoy V, Scheuer T, Catterall WA. Gating charge interactions with the S1 segment during activation of a Na+ channel voltage sensor. Proc Natl Acad Sci U S A. 2011; 108:18825–30. [PubMed: 22042870]

49. Haitin Y, et al. S1 constrains S4 in the voltage sensor domain of Kv7.1 K+ channels. PLoS One. 2008; 3:e1935. [PubMed: 18398461]

50. Yarov-Yarovoy V, et al. Structural basis for gating charge movement in the voltage sensor of a sodium channel. Proc Natl Acad Sci U S A. 2012; 109:E93–102. [PubMed: 22160714]

51. Lee SY, Banerjee A, MacKinnon R. Two separate interfaces between the voltage sensor and pore are required for the function of voltage-dependent K(+) channels. PLoS Biol. 2009; 7:e47. [PubMed: 19260762]

52. Long SB, Campbell EB, Mackinnon R. Crystal structure of a mammalian voltage-dependent Shaker family K+ channel. Science. 2005; 309:897–903. [PubMed: 16002581]

53. Pathak MM, et al. Closing in on the resting state of the Shaker K(+) channel. Neuron. 2007; 56:124–40. [PubMed: 17920020]

54. Tsutsui H, Jinno Y, Tomita A, Okamura Y. Optically detected structural change in the N-terminal region of the voltage-sensor domain. Biophys J. 2013; 105:108–15. [PubMed: 23823229]

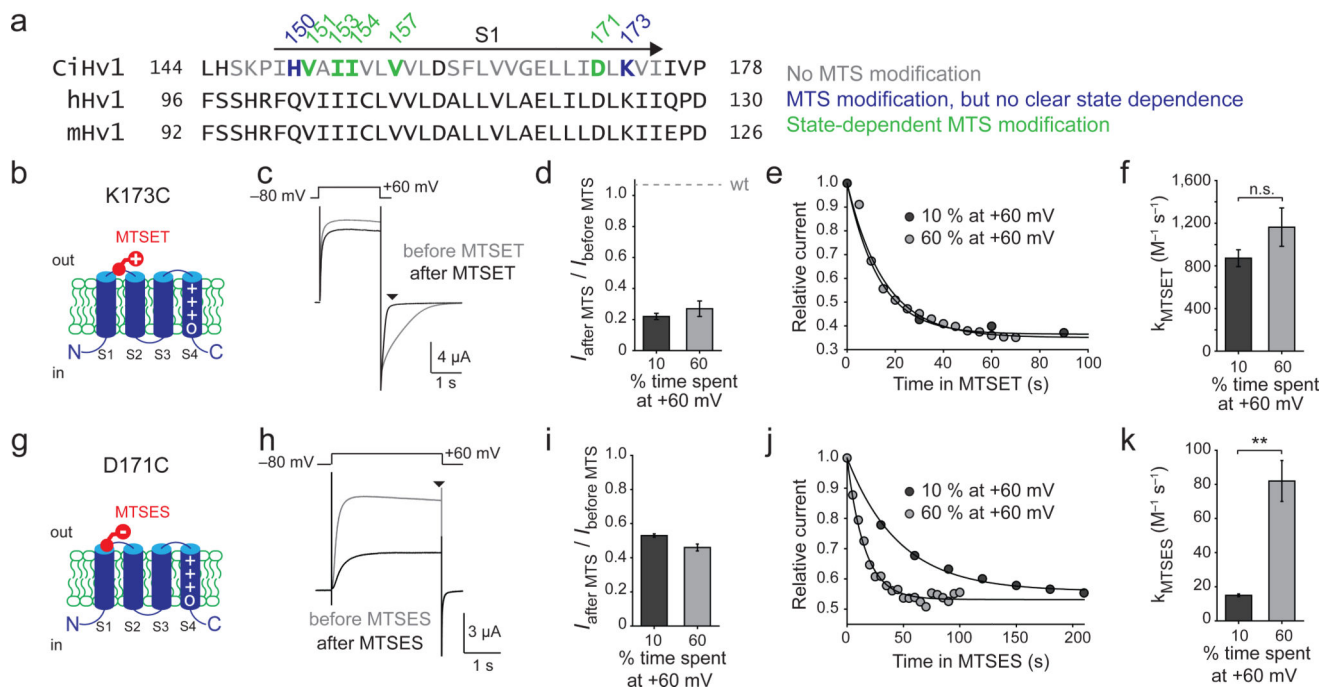55. Kohout SC, Ulbrich MH, Bell SC, Isacoff EY. Subunit organization and functional transitions in Ci-VSP. Nat Struct Mol Biol. 2008; 15:106–8. [PubMed: 18084307]

Figure 1. Weak voltage-dependence of accessibility at external end of S1
(a) S1 sequence alignment of CiHv1, human Hv1 (hHv1), and mouse Hv1 (mHv1). Color-coded letters, residues tested for MTS modification. (b-f) K173C equally accessible to external MTSET at negative and positive voltages (n = 11 and 10 oocytes for 10 % and 60 % of the time at +60 mV, respectively). (c) Current elicited by a +60 mV voltage step before (grey) and after (black) application and washout of 100 μM MTSET. (d) MTSET-induced steady-state current decrease at arrowhead in (c) (grey dashed line, wt). (e) Tail-current changes, fitted with single exponentials. (f) Rate constants of modification (10%, k_{MTSET} = 870 ± 80 M^{-1} s^{-1}; 60 %, k_{MTSET} = 1160 ± 180 M^{-1} s^{-1}; p = 0.17, two-tailed Student's t-test). (g-k) D171C more rapidly modified by external MTSES at positive voltage (n = 6 oocytes). (h) Current elicited by a +60 mV voltage step before (grey) and after (black) application and washout of 1 mM MTSES. (i) MTSES-induced steady-state current inhibition at arrowhead in (h). (j) Outward-current changes, fitted with single exponentials. (k) Rate constants of modification (10%, k_{MTSES} = 82 ± 12 M^{-1} s^{-1}; 60 %, k_{MTSES} = 15.0 ± 0.8 M^{-1} s^{-1}; p < 0.01, two-tailed Student's t-test). Error bars, s.e.m.
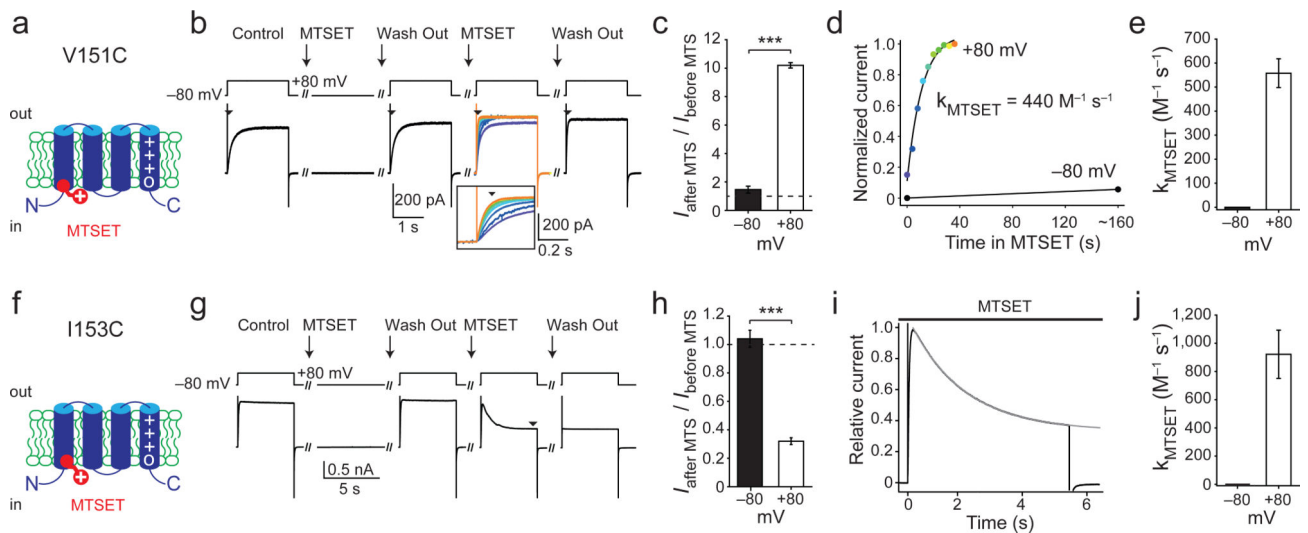
Figure 2. Strong voltage-dependence of accessibility at internal end of S1

(a-e) V151C modified by internal MTSET only at positive voltage (n = 4 patches). (b) V151C currents before (control), during application, first at –80 mV, then during repeated steps to +80 mV (chronological color code from violet to red), and after washout (at –80 mV) of 200 μM MTSET. Inset, magnification of the current traces at stimulus onset. (c) MTSET-induced steady-state current increase at arrowhead in (b), at –80 or +80 mV (p < 0.001, two-tailed Student's t-test). Dashed line, absence of effect. (d) Outward-current change at –80 or +80 mV, fitted with exponential (+80 mV) or linear (–80mV). (e) Rate constants of modification at –80 mV (k_{MTSET} = 1.6 ± 0.4 M^{-1} s^{-1}) and +80 mV (k_{MTSET} = 558 ± 60 M^{-1} s^{-1}). (f-j) I153C modified by internal MTSET only at positive voltage. (g) Currents before (control), during application, first at –80 mV, then at +80 mV, and after washout (at –80 mV) of 1 mM MTSET. (h) MTSET-induced steady-state current inhibition at –80 mV (n = 5 patches) or +80 mV (n = 6 patches), measured at arrowhead in (g) (p < 0.001, two-tailed Student's t-test). Dashed line, absence of effect. (i) Current in response to a +80 mV voltage step in presence of MTSET, with single exponential fit (grey trace). (j) Rate constant of modification at +80 mV (k_{MTSET} = 920 ± 170 M^{-1} s^{-1}). Error bars, s.e.m.
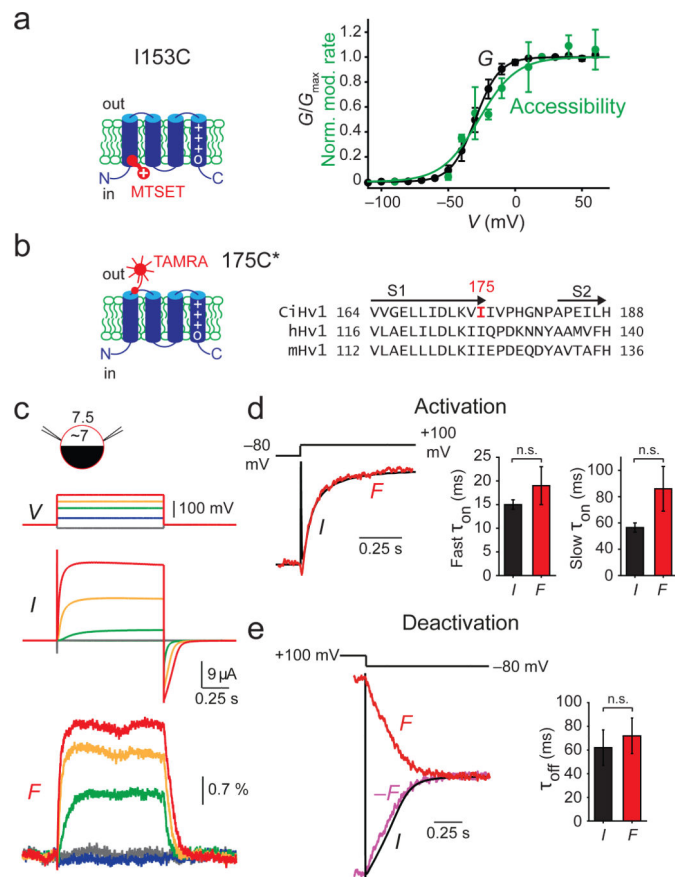
Figure 3. Environment changes around S1 are concomitant with gating

(a) Internal end: comparison of the voltage-dependence of the modification rate of I153C by MTSET (accessibility, green curve) with the voltage-dependence of I153C conductance before MTS modification (*G*, black curve). *A-V* curve (n = 3 for –20 and –10 mV data points, n = 2 for other data points), $V_{1/2} = -27 \pm 2$ mV, $kT/ze_0 = 14 \pm 3$ mV; *G-V* curve (n = 6 patches), $V_{1/2} = -30 \pm 4$ mV, $kT/ze_0 = 7.61 \pm 0.25$ mV. (b-e) VCF *F*s at outer end of S1 track opening and closing kinetics. (b) Cartoon and sequence alignment of CiHv1, hHv1, and mHv1 with TAMRA-MTS attached to I175C. (c) VCF current and fluorescence traces (as indicated in cartoon inset) of 175C* for steps from –80 mV to (in mV): grey, –100; blue, –40; green, +20; yellow, +60; red, +100. (d) Left, superposition of normalized current (black) and fluorescence (red) for a voltage step to +100 mV (activation). Right, average fast and slow activation time constants (τ_{on}) of current and fluorescence (double exponential fit; n = 14 oocytes; p = 0.39 for fast τ_{on} and 0.12 for slow τ_{on}, two-tailed paired t-tests). (e) Left, superposition of normalized current (black), fluorescence (red), and inverted fluorescence (pink) during repolarization from +100 to – 80 mV (deactivation). Right, average deactivation-time constants (τ_{off}) of current and fluorescence (single exponential fit; n = 8 oocytes; p = 0.08, two-tailed paired t-test). Error bars, s.e.m.
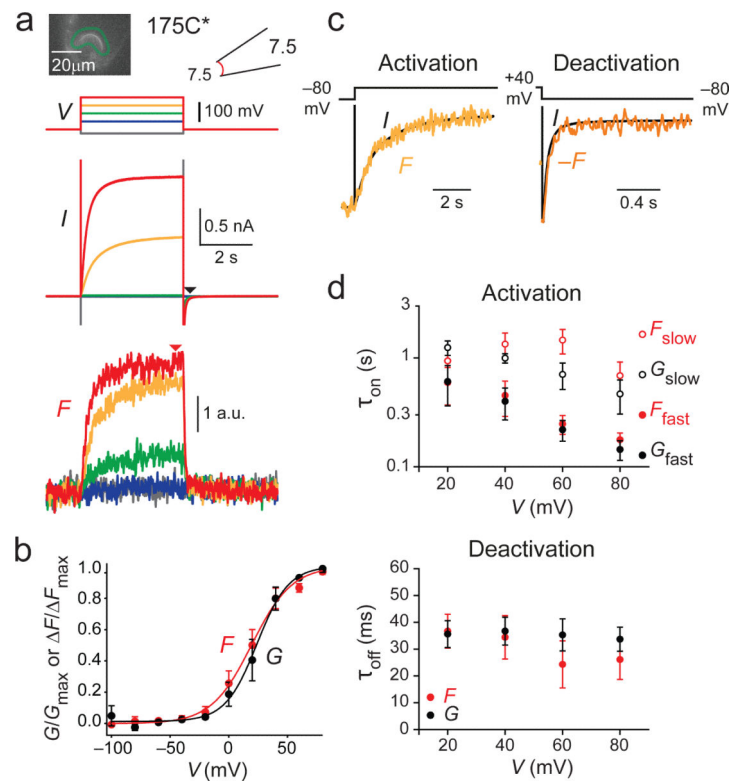
Figure 4. PCF fluorescence changes at S1 track gating

(a) PCF current and fluorescence traces of 175C* for steps from –80 mV to (in mV): grey, –100; blue, –40; green, 0; yellow, +40; red, +80. Top insets: Left, EMCCD fluorescence image of an inside-out giant patch from an oocyte expressing I175C labeled with TAMRA-MTS. Bright curved line circled in green is the voltage-clamped labeled membrane in the pipette. Right, Cartoon of fluorescent inside-out patch with internal and external pH indicated. (b) F-V (red) and G-V (black) curves (measured at arrowheads in (a)) with $V_{1/2}$ = 24 ± 6 mV, kT/ze_0 = 13.5 ± 0.9 mV (G-V), $V_{1/2}$ = 19 ± 6 mV, kT/ze_0 = 17 ± 1 mV (F-V) (n = 4 patches). (c) Superposition of the normalized current (black) and fluorescence (activation, yellow) and inverted fluorescence (deactivation, orange) for a voltage step to +40 mV (activation) and back to –80 mV (deactivation). (d) Top, average fast (closed circles) and slow (open circles) time constants of current (black) and fluorescence (red) in response to different voltage steps (activation, double exponential fits). Bottom, average current and fluorescence time constants following repolarization to –80 mV (deactivation, single exponential fits). n = 6 patches. Error bars, s.e.m.
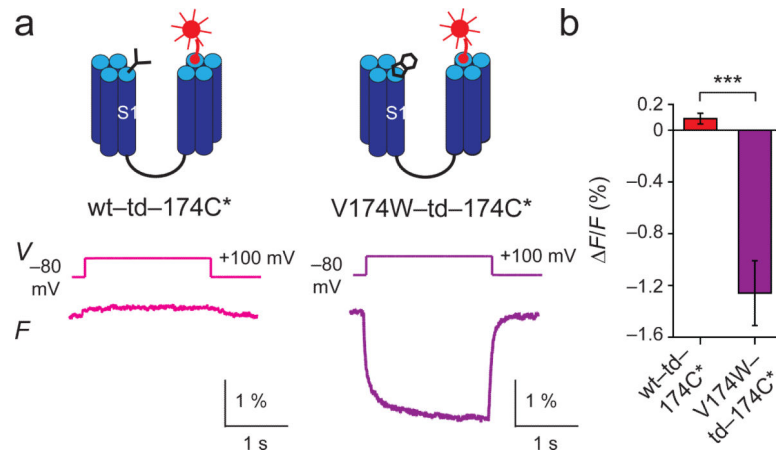
Figure 5. S1 undergoes voltage-dependent motion

(a) VCF fluorescence traces of wt-td-174C and V174W-td-174C Hv1 tandem dimers labeled with TAMRA-MTS (wt-td-174C* and V174W-td-174C*) for a step from –80 to +100 mV. Traces represent the average of 20 recordings on the same cell. (b) Magnitude of fluorescence changes of wt-td-174C* (n = 7 oocytes) and V174W-td-174C* (n = 9 oocytes). p < 0.001, two-tailed Student's t-test. Error bars, s.e.m.
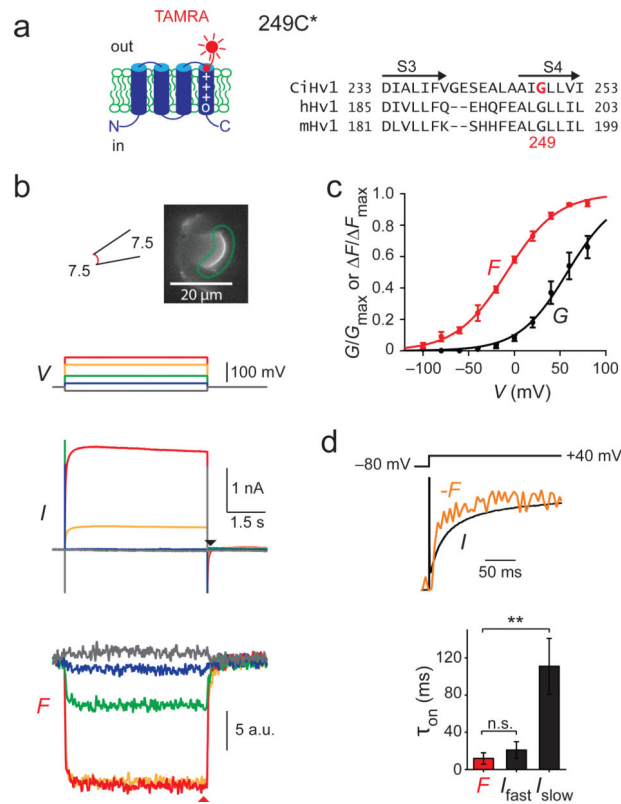
Figure 6. PCF fluorescence changes at S4 track the voltage-sensing step

(a) Cartoon and sequence alignment of CiHv1, hHv1, and mHv1. TAMRA-MTS was attached to G249C. (b) Current and fluorescence traces of 249C* for steps from –80 mV to (in mV): grey, –100; blue, –60; green, –20; yellow, +40; red, +80. Top inset, cartoon (left) and fluorescence image (right) of an inside-out giant patch containing G249C*. (c) *F-V* (red) and *G-V* (black) curves (measured at arrowheads in (b)), with $V_{1/2} = 58 \pm 9$ mV, $kT/ze_0 = 24 \pm 3$ mV (*G-V*), and $V_{1/2} = -8 \pm 2$ mV, $kT/ze_0 = 29 \pm 4$ mV (*F-V*). n = 5 patches. (d) Top, superposition of normalized current (black, double exponential fit) and inverted fluorescence (dark orange, single exponential fit) traces for a voltage step to +40 mV (activation). Bottom, average time constant of fluorescence, and fast (I_{fast}) and slow (I_{slow}) time constants of current during a voltage step to +40 mV. n = 6 oocytes; n.s., p = 0.94; **, p < 0.01, One-way ANOVA followed by Tukey test. Error bars, s.e.m.
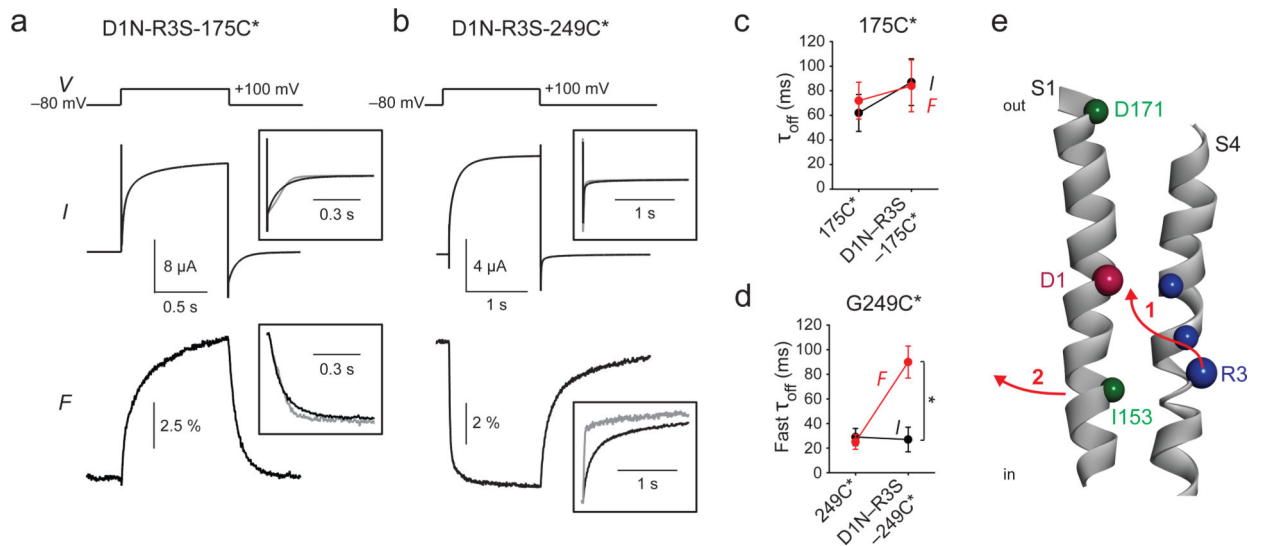
Figure 7. Neutralization of D1 and R3 has differential effects on S1 and S4 *F*s

(a-b) VCF current and fluorescence traces of D1N-R3S-175C* (a, S1 motion) and D1N-R3S-249C* (b, S4 motion). Insets, superposition of normalized deactivation current and fluorescence of 175C* (a) or 249C* (b) with (black) or without (grey) D1N-R3S mutations. (c) No significant changes in deactivation time constants (τ_{off}) between 175C* (n = 8 oocytes) and D1N-R3S-175C* (n = 5 oocytes). Current, p = 0.34; fluorescence, p = 0.63; two-tailed Student's t-tests. No significant changes in τ_{off} between current and fluorescence (175C*, p = 0.08; D1N-R3S-175C*, p = 0.49; two-tailed paired t-tests). (d) Significant changes in fast deactivation time constants (fast τ_{off}) of fluorescence (p = 0.002) but not current (p = 0.63) between 249C* (n = 9 oocytes) and D1N-R3S-249C* (n = 7 oocytes). Two-tailed Student's t-tests. Significant changes in fast τ_{off} between current and fluorescence in D1N-R3S-249C* (p = 0.02) but not in 249C* (p = 0.12). Two-tailed paired t-tests. (e) Proposed molecular motions that gate Hv1. Arrangement of S1 and S4 segments from the mHv1cc crystal structure[31] (putative resting state), with marked key residues D1 (pink), S4's arginines (blue), and two S1 residues, D171 and I153 (green). Arrows, putative S4 and S1 motions during gating. 1, voltage-sensing: outward motion and rotation of S4 to place R3 in register with D1. 2, opening: rearrangement of S1, which opens a wide intracellular cavity, allowing access to the D1-R3 selectivity filter. Error bars, s.e.m.